



# CHORUS

This is the accepted manuscript made available via CHORUS. The article has been published as:

## Bose-Hubbard Models with Synthetic Spin-Orbit Coupling: Mott Insulators, Spin Textures, and Superfluidity

William S. Cole, Shizhong Zhang, Arun Paramekanti, and Nandini Trivedi

Phys. Rev. Lett. **109**, 085302 — Published 20 August 2012

DOI: [10.1103/PhysRevLett.109.085302](https://doi.org/10.1103/PhysRevLett.109.085302)

# Bose Hubbard Models with Synthetic Spin-Orbit Coupling: Mott Insulators, Spin Textures and Superfluidity

William S. Cole,<sup>1</sup> Shizhong Zhang,<sup>1</sup> Arun Paramekanti,<sup>2,3</sup> and Nandini Trivedi<sup>1</sup>

<sup>1</sup>*Department of Physics, The Ohio State University, Columbus OH 43210, USA*

<sup>2</sup>*Department of Physics, University of Toronto, Toronto M5S1A7, Canada*

<sup>3</sup>*Canadian Institute for Advanced Research, Toronto, Ontario, M5G 1Z8, Canada*

(Dated: July 3, 2012)

Motivated by the experimental realization of synthetic spin-orbit coupling for ultracold atoms, we investigate the phase diagram of the Bose Hubbard model in a non-abelian gauge field in two dimensions. Using a strong coupling expansion in the combined presence of spin-orbit coupling and tunable interactions, we find a variety of interesting magnetic Hamiltonians in the Mott insulator (MI), which support magnetic textures such as spin spirals and vortex and Skyrmion crystals. An inhomogeneous mean field treatment shows that the superfluid (SF) phases inherit these exotic magnetic orders from the MI and display, in addition, unusual modulated current patterns. We present a slave boson theory which gives insight into such intertwined spin-charge orders in the SF, and discuss signatures of these orders in Bragg scattering, *in situ* microscopy, and dynamic quench experiments.

*Introduction.*—Strong spin-orbit (SO) interaction is key to realizing remarkable states of electronic matter, such as topological band insulators [1, 2] and Weyl semimetals [3]. SO coupled Mott insulators can realize the Kitaev model [4] which may enable the study of Majorana fermions in a condensed matter setting and provide a platform for topological quantum computation [5]. This has motivated parallel experimental advances in ultracold atomic gases, where Raman processes can be used to create tunable SO coupling, or more general nonabelian gauge fields [6–8], paving the way to investigating SO coupling and its emergent consequences for atomic gases.

Experiments [6–9] and theory [10–16] on SO coupled bosons have mainly focused on Bose-Einstein condensation in *weakly* interacting gases without a lattice potential. However, as theory [17–19] and experiments [20] without SO interaction have shown, tuning the lattice depth for bosons in an optical lattice can lead to a strongly interacting regime, accompanied by a suppression of the condensate density and finally a quantum phase transition into a featureless Mott insulator [21]. By contrast the physics of SO coupled atoms in an optical lattice, both of which are expected to lead to unique phenomena, remains a relatively unexplored frontier [22].

In this Letter we demonstrate that tuning SO coupling and interparticle interactions for ‘spinful’ bosons at a filling of one boson per site leads to Mott insulating states with a plethora of magnetic Hamiltonians including Dzyaloshinskii-Moriya (DM) interactions [23, 24]. This provides a toolbox to simulate several interesting quantum magnetic models. These effective Hamiltonians on a two-dimensional (2D) square lattice are shown to have a rich classical phase diagram, exhibiting Ising and XY ferromagnets, an Ising antiferromagnet, two coplanar spiral phases, and vortex and Skyrmion crystals. In contrast to solid state materials, it is easier to tune across

this phase diagram by varying experimental parameters. Upon increasing the boson tunneling, we find superfluid phases that inherit magnetic textures from the underlying Mott state. We then formulate a slave boson approach that provides a unified understanding of the spin-charge orders in the SF phase, as well as the SF-MI transitions. We conclude by discussing experimental predictions which emerge from our theory.

*Model.*—We consider bosons with two hyperfine states ( $\uparrow$  and  $\downarrow$ ), described by the following Hamiltonian on a 2D square lattice:

$$H = -t \sum_{\langle ij \rangle} (\psi_i^\dagger \mathcal{R}_{ij} \psi_j + \text{h.c.}) + \frac{1}{2} \sum_{i\sigma\sigma'} U_{\sigma\sigma'} a_{i\sigma}^\dagger a_{i\sigma'}^\dagger a_{i\sigma'} a_{i\sigma} \quad (1)$$

where  $\psi_i^\dagger = (a_{i\uparrow}^\dagger, a_{i\downarrow}^\dagger)$ , and  $a_{i\sigma}^\dagger$  creates a spin- $\sigma$  boson at site  $i$ . The first term describes tunneling of bosons between neighboring sites, with  $t$  the overall hopping amplitude. The matrix  $\mathcal{R}_{ij} \equiv \exp[i\vec{A} \cdot (\vec{r}_i - \vec{r}_j)]$ , where  $\vec{A} = (\alpha\sigma_y, \beta\sigma_x, 0)$  is a *non-abelian* background gauge field seen by the bosons. Diagonal terms in this matrix describe spin-conserving hopping of bosons, while off-diagonal spin-flip terms describe the SO coupling arising from a two-photon Raman process [25]. We set  $\beta = -\alpha$ , for which the SO coupling is the lattice analog of the well-known Rashba term. The second term describes boson interactions; we choose the intraspecies repulsion  $U_{\uparrow\uparrow} = U_{\downarrow\downarrow} \equiv U$ , and set the interspecies interaction  $U_{\uparrow\downarrow} = U_{\downarrow\uparrow} \equiv \lambda U$ .

We analyze this model using various methods: (i) a weak coupling ( $U, \lambda U \ll t$ ) Gross-Pitaevskii approach to study the condensate structure; (ii) a strong coupling ( $U, \lambda U \gg t$ ) approach to understand the Mott state and associated spin textures; (iii) an inhomogeneous mean field theory to describe the emergent strongly correlated superfluids; (iv) a ‘‘slave-boson’’ theory to understand the coupled magnetic and charge orders.

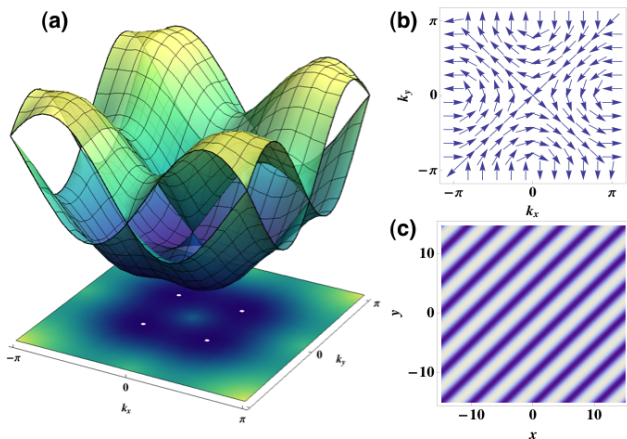


FIG. 1. (Color online) (a) Band structure of Eq. (1) for  $U = 0$ , with  $\alpha = -\beta = \pi/4$ . There are four degenerate minima at  $\vec{Q}_1, \dots, \vec{Q}_4$  in the lower band due to rotational symmetry breaking by the square lattice and a Dirac cone at the  $\Gamma$  point. (b) The spin eigenstates in the lower band. The spin is locked to the momentum through the SO coupling. (c) Real-space density distribution of spin-up particles in the condensate with  $\lambda = 1.3$  from the GP calculation. There is a similar distribution for the spin-down particles. On the other hand, for  $\lambda < 1$ , the spin density is uniform. The *total* density is uniform for all  $\lambda$ .

*Weak coupling superfluid.*—The non-interacting band structure for Eq. (1), shown in Fig. 1(a), has four degenerate minima in the lower band at  $\vec{Q}_1 = (k_0, k_0)$ ,  $\vec{Q}_2 = (-k_0, k_0)$ ,  $\vec{Q}_3 = (-k_0, -k_0)$  and  $\vec{Q}_4 = (k_0, -k_0)$ , where  $\tan k_0 = (\tan \alpha)/\sqrt{2}$ . This contrasts sharply with the continuum case where the minima form a degenerate circle, and suggests that Rashba coupled condensates confined to an optical lattice are more stable against fluctuations. We label the eigenstates at these points as  $\varphi_m = \exp(i\vec{Q}_m \cdot \vec{r})\chi_m$ ,  $m = 1, \dots, 4$ . The spin wavefunction  $\chi_m$  associated with  $\varphi_m$  has the form  $\chi_m^\dagger \equiv (1/\sqrt{2})(1, \exp(-im\pi/4))$ , and more generally winds around the  $\Gamma$  point in the first Brillouin zone with a winding number 1, as shown in Fig. 1(b).

Within the Gross-Pitaevskii (GP) approximation, all  $N$  bosons condense into a common single particle state  $\Phi = \sum_m c_m \varphi_m$  where  $c_m$  are complex variational parameters, satisfying  $\sum_m |c_m|^2 = 1, m = 1, \dots, 4$ . Setting  $\Phi^\dagger \equiv (\Phi_\uparrow^*, \Phi_\downarrow^*)$ , we determine  $c_m$  by minimizing the interaction energy  $U_{\text{int}}(\{c_m\}) \equiv NU/2(|\Phi_\uparrow|^4 + |\Phi_\downarrow|^4 + 2\lambda|\Phi_\uparrow|^2|\Phi_\downarrow|^2)$  [26]. As an illustration, for  $\alpha = \pi/4$  we find the following behavior: For  $\lambda < 1$ , only one of the four states is occupied. In this case, both the spin and number density of the superfluid are uniform, and the ground state is four-fold degenerate. For  $\lambda > 1$ , two states with opposite wave vectors are occupied, leading to stripe order in the spin density (see Fig. 1(c)) while

TABLE I. Exchange couplings in the effective hamiltonian. Taking  $\alpha$  and  $\lambda$  as tunable parameters, several quantum magnetic Hamiltonians can be realized.

$J_{\hat{x}}^x = -\frac{4t^2}{\lambda U} \cos(2\alpha)$	$J_{\hat{y}}^x = -\frac{4t^2}{\lambda U}$
$J_{\hat{x}}^y = -\frac{4t^2}{\lambda U}$	$J_{\hat{y}}^y = -\frac{4t^2}{\lambda U} \cos(2\alpha)$
$J_{\hat{x}}^z = -\frac{4t^2}{\lambda U} (2\lambda - 1) \cos(2\alpha)$	$J_{\hat{y}}^z = -\frac{4t^2}{\lambda U} (2\lambda - 1) \cos(2\alpha)$
$\vec{D}_{\hat{x}} = -\frac{4t^2}{U} \sin(2\alpha) \hat{y}$	$\vec{D}_{\hat{y}} = \frac{4t^2}{U} \sin(2\alpha) \hat{x}$

the total density remains uniform. The wave vector for the spin-stripe density is  $2\sqrt{2}k_0$  and the ground state is two-fold degenerate. Similar magnetic states are found below at strong coupling, but this GP approach focusing on the minima at  $\vec{Q}_m$  misses the additional magnetic textures.

*Strong coupling Mott phases.*—At unit filling and for  $U/t = \infty$ , repulsive interactions favor exactly one boson at each site. The ground states at  $t = 0$  are highly degenerate, with an arbitrary spin state at each site. Away from this limit, to  $\mathcal{O}(t^2/U)$ , we obtain the effective low-energy spin Hamiltonian

$$H_{\text{spin}} = \sum_{i, \delta=\hat{x}, \hat{y}} \left\{ \sum_{a=x, y, z} J_{\delta}^a S_i^a S_{i+\delta}^a + \vec{D}_{\delta} \cdot (\vec{S}_i \times \vec{S}_{i+\delta}) \right\} \quad (2)$$

where the exchange coupling constants  $J_{\delta}^a$  and DM vectors  $\vec{D}_{\delta}$  are given in Table I. Thus, by tuning  $\alpha$  and  $\lambda$  in a single system, one can emulate several Hamiltonians of interest in quantum magnetism. For example, for  $\alpha=0$ ,  $H_{\text{spin}}$  reduces to an XXZ magnet [27] with negative (ferromagnetic)  $xy$ -coupling and a  $z$ -coupling determined by  $(1 - 2\lambda)$ . For  $\alpha \neq 0$ , one obtains both anisotropic exchange couplings as well as a DM interaction which tends to induce spin spirals as in chiral magnets like MnSi. For  $\alpha = \pi/4$  we find a “compass”-type model with a DM perturbation. The Hamiltonian in Eq. (1) thus constitutes perhaps the simplest itinerant model with chiral magnetic ground states.

We obtain the classical ground-state phase diagram of  $H_{\text{spin}}$  in Eq.(2) via Monte Carlo annealing [28] (see Fig. 2). We find the following phases characterized by a magnetic structure factor  $S_{\vec{q}} = |\sum_i \vec{S}_i e^{i\vec{q} \cdot \vec{r}_i}|$ .

**xyFM/zFM:** Ferromagnetic phases where the spin structure factor exhibits a peak at  $\vec{q} = (0, 0)$ . In the zFM, spins orient along the  $\pm z$ -axis. In the xyFM, the SO interaction pins the spins to lie in the  $xy$ -plane making angles  $(2n + 1)\pi/4$  (with  $n = 0 \dots 3$ ) with the  $x$ -axis.

**zAFM:** Antiferromagnetic phase where  $S_{\vec{q}}$  exhibits a peak at  $(\pi, \pi)$ , with spins pointing along the  $\pm z$ -axis.

**Spiral-1:** A coplanar state; spins spiral in the plane defined by the vectors  $\hat{z} - \vec{q}$ , where  $\vec{q} \equiv (q, \pm q)$  is an incommensurate wavevector.

**Spiral-2:** A coplanar state, with spins spiralling in the  $\hat{z} - \vec{q}$  plane, where  $\vec{q} \equiv (q, 0)$  (or  $(0, q)$ ) is incommensurate for small  $\alpha$ , but there is a parameter region (light green

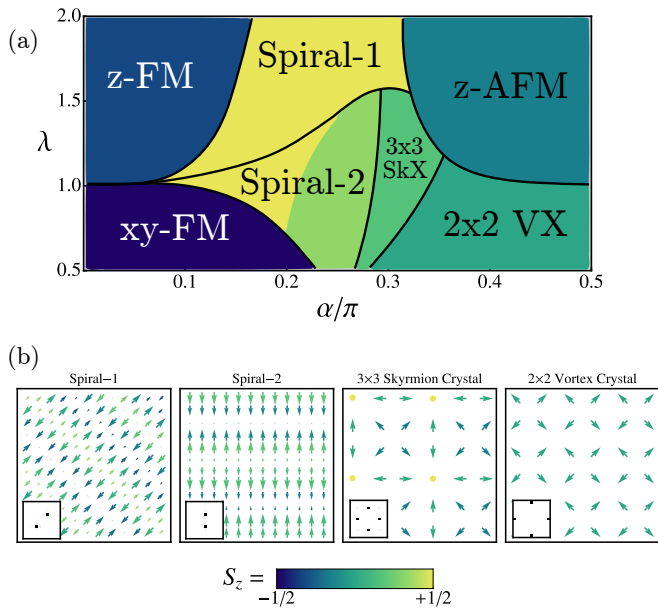


FIG. 2. (Color online) (a) Phase diagram in the Mott insulating regime from Monte Carlo annealing of the spin hamiltonian Eq. (2). Spin configurations are abbreviated as described in the text. The darker area of the Spiral-2 region represents a commensurate 4-site spiral. (b) shows the  $xy$ -plane projection of the real space spin configurations in the Spiral-1, 2, SkX, and VX phases. The magnetic structure factor peaks are shown in the insets.

region of “Spiral-2” in Fig. 2) that supports a commensurate  $(4 \times 1)$ -site unit cell.

**$2 \times 2$  Vortex Crystal (VX):** A coplanar ground state, with spins in the  $xy$ -plane having components  $S_x = (-1)^x/\sqrt{2}$  and  $S_y = (-1)^y/\sqrt{2}$ . The spins wind clockwise or counterclockwise around each plaquette. The VX has  $S_{\vec{q}}$  peaks at  $(\pi, 0)$  and  $(0, \pi)$ .

**$3 \times 3$  Skyrmion Crystal (SkX):** A *non-coplanar* state, where the spins form a  $3 \times 3$  unit cell with nonzero Skyrmion density, given by  $\sum_i \vec{S}_i \cdot (\vec{S}_{i+\hat{x}} \times \vec{S}_{i+\hat{y}})$ . The structure factor has peaks at  $(2\pi/3, 0)$  and  $(0, 2\pi/3)$ .

The Spiral-1, Spiral-2, VX, and SkX phases break the  $C_{4v}$  symmetry of the square lattice; they are thus expected to undergo multiple thermal transitions, associated with restoring spin rotational and lattice rotational symmetries, enroute to the high temperature paramagnetic state. In the Spiral-1 phase, for example, these transitions are manifested through two specific heat peaks in our classical Monte Carlo simulations [29].

*Mott lobes and magnetically textured SFs.*—To address the strongly correlated superfluid phases beyond the GP approach, and to connect with the magnetic textures in the Mott insulator, we extend the numerical mean field theory introduced in [30] to spinful bosons.

We introduce the order parameter  $\phi_{i\sigma} = \langle a_{i\sigma} \rangle$  and decompose the kinetic term of the Hamiltonian in Eq.(1) as  $a_{i\sigma}^\dagger a_{j\sigma'} \approx a_{i\sigma}^\dagger \phi_{j\sigma'} + \phi_{i\sigma}^* a_{j\sigma'} - \phi_{i\sigma}^* \phi_{j\sigma'}$ , where terms quadratic in the fluctuations have been discarded. In order to capture non-uniform magnetic ordering, and possible inhomogeneous superfluidity, we must allow for a spatially varying condensate order parameter. The self-consistent solution of this mean field theory requires an iterative minimization over a finite cluster (more details are given in [28]).

For  $t = 0$ , the single site Hamiltonian is  $H_U = (U/2)(n_\uparrow^2 + n_\downarrow^2 + 2\lambda n_\uparrow n_\downarrow) - (\mu + U/2)(n_\uparrow + n_\downarrow)$ . Thus, the maximum size of the Mott lobe is  $\min(U, \lambda U)$  along the  $\mu$ -axis. As we increase  $t/U$ , there is a quantum phase transition from the magnetic insulating states to the superfluid states at a critical value  $(t/U)_c$ , which increases with  $\alpha$  for fixed  $\lambda$ . This is consistent with previous results obtained using a hopping expansion [22] which, however, only addressed the homogeneous Mott phase with xyFM magnetic order.

To characterize the magnetic structures in the superfluid phase, we calculate (i) the local magnetic moment  $\vec{m}_i \equiv \langle a_{i\mu}^\dagger \vec{\sigma}_{\mu\nu} a_{i\nu} \rangle$  and (ii) the bond current  $\kappa_{ij}^{\mu\nu} = -it(\mathcal{R}_{ij}^{\mu\nu} \langle a_{i\mu}^\dagger a_{j\nu} \rangle - c.c.)$ , where  $ij$  are nearest neighbors. For the phases we now describe, the diagonal term  $\mu = \nu$  of  $\kappa_{ij}^{\mu\nu}$  is zero and the nonzero off-diagonal term represents the total current arising from spin flip processes.

In Fig.3 (A) and (B), we plot the Mott lobes for filling  $n = 1$  and  $\alpha = \pi/2$ , together with the  $z$ -component of the onsite spin density and bond currents in the SF phase. We find that for  $\lambda = 1.5$  and  $\lambda = 0.5$  the magnetic order in the SF reflects the magnetic order in the underlying Mott state. In addition the SFs support a checkerboard pattern of plaquette currents. We find for  $\lambda = 1.5$ , where the Mott phase is zAFM, this current order spontaneously breaks the time reversal symmetry (in picking one of the two allowed checkerboard patterns), while for  $\lambda = 0.5$ , the underlying magnetic phase picks a unique loop current order. To understand this interplay between magnetic order and bond current patterns found in our inhomogeneous mean-field theory, we next formulate a slave boson theory of this problem which also provides a unified framework to understand the SF-MI transitions.

*Slave boson theory.*—Inspired by theories of strongly correlated electronic materials [31, 32], we decompose the physical boson  $a$  into separate bosonic spin and charge degrees of freedom:  $a_{i,\sigma}^\dagger = \frac{1}{\sqrt{\hat{n}_{b,i}}} b_i^\dagger f_{i,\sigma}^\dagger$ , where the  $b$ -bosons (chargons) carry charge but no spin, while the  $f$ -bosons (spinons) carry spin but no charge. The physical Hilbert space of the  $a$ -bosons is given by specifying the number of up- and down-spin  $a$ -bosons on each lattice site  $|m \uparrow, \ell \downarrow\rangle$ . On the other hand, in the slave-particle representation, we write these states as

$$|m \uparrow, \ell \downarrow\rangle_a = |(m + \ell)_b \otimes |m \uparrow, \ell \downarrow\rangle_f \quad (3)$$

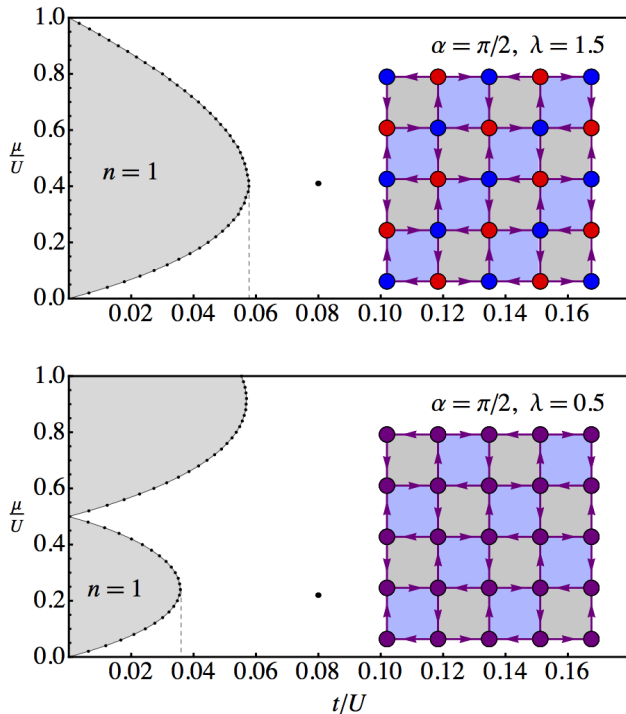


FIG. 3. (Color online) Phase diagrams of the spin-orbit coupled Bose-Hubbard model in  $\mu/U$  vs.  $t/U$  plane, showing Mott lobes and superfluid states. (A) phase diagram with  $\lambda = 1.5$  and  $\alpha = \pi/2$  and (B)  $\lambda = 0.5$  and  $\alpha = \pi/2$ . The width of the  $n = 1$  lobe is given by  $\lambda U$  and the critical value  $(t/U)_c$  increases with  $\lambda$ . The two insets show the local spin density distribution (red= $\uparrow$ , blue= $\downarrow$ , purple in between) and bond currents for  $t/U = 0.08$  in the superfluid phase close to the Mott states.  $\mu/U$  is tuned such that the average number of particles per site is unity. For  $\lambda = 1.5$ , the spin density assumes  $z$ -antiferromagnetic order whereas for  $\lambda = 0.5$ , the magnetic moments are in the  $2 \times 2$  VX phase, and restricted to the  $xy$ -plane. The bond currents for both  $\lambda = 1.5$  and  $\lambda = 0.5$  share the same pattern, with clockwise and anti-clockwise plaquette loop currents forming Ising anti-ferromagnetic order.

In this approach, the  $b$  and  $f$  operators can act on the right hand side independently. To remain in the physical Hilbert space of the problem, we must impose the local constraint  $b_i^\dagger b_i = \sum_\sigma f_{i\sigma}^\dagger f_{i\sigma}$ . At mean-field level, this constraint is treated on average and we are led to two separate, coupled Hamiltonians for the spinons and chargons which need to be solved self-consistently [28].

We want to understand the superfluid phases with magnetic textures as indicated by the inhomogeneous mean-field results. The magnetic textures can be obtained by condensing the spinons into an appropriate condensate wavefunction  $\Phi_{i\sigma}$ . This leads to an effective chargon Hamiltonian

$$H_b = -t \sum_{\langle ij \rangle \mu \nu} (R_{ij}^{\mu\nu} \Phi_{i\mu}^* \Phi_{j\nu} b_i^\dagger b_j + \text{h.c.}) + \frac{U}{2} \sum_i b_i^\dagger b_i^\dagger b_i b_i. \quad (4)$$

Different magnetic textures thus ‘act’ on the chargons as

distinct effective *abelian* gauge field configurations.

As a simple example, consider the magnetic order in the zFM which is captured by setting  $\Phi_{i\uparrow} = 1$  and  $\Phi_{i\downarrow} = 0$ . This leads to a conventional Bose Hubbard model for the chargons, but with a renormalized chargon hopping amplitude  $t \cos \alpha$ . This renormalizes the critical interaction needed to drive the Mott transition at unit filling from  $U_c^0$  for spinless bosons to  $U_c^{zFM}(\alpha) = U_c^0 \cos \alpha$ . Going beyond mean field theory, we conclude that this Mott transition remains in the 3D-XY universality class [29].

To understand the bond current ordered SF emerging from the insulator with zAFM order, we set  $\Phi_{r\uparrow} = 1$  and  $\Phi_{r\downarrow} = 0$  on the A sublattice, and  $\Phi_{r\downarrow} = 1$  and  $\Phi_{r\uparrow} = 0$  on the B sublattice. Compared to the previous case, the chargon Hamiltonian is now seen to enclose  $\pi$ -flux per plaquette for the chargons. This flux results in the spontaneous checkerboard pattern [33, 34] of mass currents seen in Fig.3 (A). The SF phases emerging from the SkX, VX, Spiral-1 and Spiral-2 phases, as well as a complete SB mean field theory, treating magnetic and charge orders self-consistently, will be discussed elsewhere [29].

*Experimental implications.*—One interesting aspect of our work is the realization that one can tune across a wide variety of magnetic Hamiltonians, which support magnetically textured Mott insulators and superfluids, starting from the simple Bose Hubbard model in Eq. (1). The magnetic structure factor in the different phases, shown in Fig.2, can be directly measured with optical Bragg scattering experiments [35].

Another route to exploring these ordered phases is via *in situ* microscopy which can detect lattice-resolved hyperfine states and number fluctuations of atoms [36]. Finally, the unusual bond currents in the SF phases, such as the checkerboard current pattern in the SF phase descending from the zAFM, could be detected using a recent proposal to quench the lattice potential along one direction which dynamically converts these current patterns into measurable atomic density patterns [37]. Such experiments would provide a deeper understanding of the emergent consequences of the interplay of spin-orbit coupling and strong interactions for bosons.

We thank J. Radić, A. Di Ciolo, K. Sun, and V. Galitski for discussions and comparing data on the classical magnetic phases. We acknowledge funding from ARO Grant W911NF-08-1-0338 (W.S.C), DARPA under the Optical Lattice Emulator program R15835 (S.Z.) and NSF DMR-0907275 (N.T.). A.P. acknowledges support from NSERC (Canada).

*Note added.* During the completion of this work, we become aware of the complementary work by Radić *et al.* [38]. Where our results overlap, they are in agreement.

- 
- [1] M. Hasan and C. Kane, *Reviews Of Modern Physics* **82**, 3045 (2010).
- [2] X.-L. Qi and S.-C. Zhang, *Reviews Of Modern Physics* **83**, 1057 (2011).
- [3] X. Wan, A. M. Turner, A. Vishwanath, and S. Y. Savrasov, *Phys. Rev. B* **83**, 205101 (2011).
- [4] A. Kitaev, *Annals Of Physics* **321**, 2 (2006).
- [5] G. Jackeli and G. Khaliullin, *Physical Review Letters* **102**, 017205 (2009).
- [6] Y. J. Lin, R. L. Compton, A. R. Perry, W. D. Phillips, J. V. Porto, and I. B. Spielman, *Physical Review Letters* **102**, 130401 (2009).
- [7] Y. J. Lin, R. L. Compton, K. Jiménez-García, J. V. Porto, and I. B. Spielman, *Nature* **462**, 628 (2009).
- [8] Y. J. Lin, K. Jiménez-García, and I. B. Spielman, *Nature* **471**, 83 (2011).
- [9] S. Chen, J.-Y. Zhang, S.-C. Ji, Z. Chen, L. Zhang, Z.-D. Du, Y. Deng, H. Zhai, and J.-W. Pan, *ArXiv e-prints* (2012), arXiv:1201.6018 [cond-mat.quant-gas].
- [10] H. Hu, B. Ramachandhran, H. Pu, and X.-J. Liu, *Phys. Rev. Lett.* **108**, 010402 (2012).
- [11] T. D. Stanescu, B. Anderson, and V. Galitski, *Physical Review A* **78**, 023616 (2008).
- [12] T.-L. Ho and S. Zhang, *Physical Review Letters* **107**, 150403 (2011).
- [13] C. Wang, C. Gao, C.-M. Jian, and H. Zhai, *Phys. Rev. Lett.* **105**, 160403 (2010).
- [14] W. Cong-Jun, I. Mondragon-Shem, and Z. Xiang-Fa, *Chinese Physics Letters* **28**, 097102 (2011).
- [15] T. Ozawa and G. Baym, *Phys. Rev. A* **85**, 013612 (2012).
- [16] Y. Zhang, L. Mao, and C. Zhang, *Phys. Rev. Lett.* **108**, 035302 (2012).
- [17] M. P. A. Fisher, P. B. Weichman, G. Grinstein, and D. S. Fisher, *Physical Review B* **40**, 546 (1989).
- [18] D. Jaksch, C. Bruder, J. I. Cirac, C. W. Gardiner, and P. Zoller, *Phys. Rev. Lett.* **81**, 3108 (1998).
- [19] E. Altman, W. Hofstetter, E. Demler, and M. D. Lukin, *New Journal of Physics* **5**, 113 (2003).
- [20] M. Greiner, O. Mandel, T. Esslinger, T. W. Hänsch, and I. Bloch, *Nature* **415**, 39 (2002).
- [21] S. Sachdev, *Quantum Phase Transitions* (Cambridge University Press, 2011).
- [22] T. Graß, K. Saha, K. Sengupta, and M. Lewenstein, *Physical Review A* **84**, 053632 (2011).
- [23] I. Dzyaloshinskii, *Journal Of Physics And Chemistry Of Solids* **4**, 241 (1958).
- [24] T. Moriya, *Physical Review* **120**, 91 (1960).
- [25] K. Osterloh, M. Baig, L. Santos, P. Zoller, and M. Lewenstein, *Physical Review Letters* **95**, 010403 (2005).
- [26] For repulsive interactions, we have verified that the Gross-Pitaevskii state is energetically favored over a fragmented state..
- [27] L.-M. Duan, E. Demler, and M. D. Lukin, *Phys. Rev. Lett.* **91**, 090402 (2003).
- [28] See Supplementary Material for details.
- [29] W. S. Cole, S. Zhang, A. Paramekanti, and N. Trivedi, manuscript in preparation.
- [30] K. Sheshadri, H. R. Krishnamurthy, R. Pandit, and T. V. Ramakrishnan, *Europhysics Letters (EPL)* **22**, 257 (1993).
- [31] P. A. Lee, N. Nagaosa, and X.-G. Wen, *Reviews of Modern Physics* **78**, 17 (2006).
- [32] D. Pesin and L. Balents, *Nature Physics* **6**, 376 (2010).
- [33] L.-K. Lim, C. M. Smith, and A. Hemmerich, *Phys. Rev. Lett.* **100**, 130402 (2008).
- [34] A. Dhar, M. Maji, T. Mishra, R. V. Pai, S. Mukerjee, and A. Paramekanti, *Phys. Rev. A* **85**, 041602 (2012).
- [35] T. A. Corcovilos, S. K. Baur, J. M. Hitchcock, E. J. Mueller, and R. G. Hulet, *Physical Review A* **81**, 013415 (2010).
- [36] C. Weitenberg, M. Endres, J. F. Sherson, M. Cheneau, P. Schausz, T. Fukuhara, I. Bloch, and S. Kuhr, *Nature* **471**, 319 (2011).
- [37] M. Killi and A. Paramekanti, *Phys. Rev. A* **85**, 061606 (2012).
- [38] J. Radic, A. Di Ciolo, K. Sun, and V. Galitski, *ArXiv e-prints* (2012), arXiv:1205.2110 [cond-mat.quant-gas].